ADVANCED ELECTRONIC MATERIALS
www.advelectronicmat.de

Near-Unity Molecular Doping Efficiency in Monolayer MoS_2

*Milad Yarali, Yiren Zhong, Serrae N. Reed, Juefan Wang, Kanchan A. Ulman, David J. Charboneau, Julia B. Curley, David J. Hynek, Joshua V. Pondick, Sajad Yazdani, Nilay Hazari, Su Ying Quek, Hailiang Wang, and Judy J. Cha**

Surface functionalization with organic electron donors (OEDs) is an effective doping strategy for 2D materials, which can achieve doping levels beyond those possible with conventional electric field gating. While the effectiveness of surface functionalization has been demonstrated in many 2D systems, the doping efficiencies of OEDs have largely been unmeasured, which is in stark contrast to their precision syntheses and tailored redox potentials. Here, using monolayer MoS_2 as a model system and an organic reductant based on 4,4′-bipyridine (DMAP-OED) as a strong organic dopant, it is established that the doping efficiency of DMAP-OED to MoS_2 is in the range of 0.63 to 1.26 electrons per molecule. The highest doping levels to date are also achieved in monolayer MoS_2 by surface functionalization and demonstrate that DMAP-OED is a stronger dopant than benzyl viologen, which is the previous best OED dopant. The measured range of the doping efficiency is in good agreement with the values predicted from first-principles calculations. This work provides a basis for the rational design of OEDs for high-level doping of 2D materials.

Dr. M. Yarali, S. N. Reed, D. J. Hynek, J. V. Pondick, Dr. S. Yazdani, Prof. J. J. Cha
Department of Mechanical Engineering and Materials Science
Yale University
New Haven, CT 06511, USA
E-mail: judy.cha@yale.edu

Dr. M. Yarali, Y. Zhong, S. N. Reed, D. J. Hynek, J. V. Pondick, Dr. S. Yazdani, Prof. H. Wang, Prof. J. J. Cha
Energy Sciences Institute
Yale West Campus
West Haven, CT 06516, USA

Y. Zhong, D. J. Charboneau, J. B. Curley, Prof. H. Wang, Prof. N. Hazari
Department of Chemistry
Yale University
New Haven, CT 06511, USA

J. Wang, Dr. K. A. Ulman, Prof. S. Y. Quek
Department of Physics
National University of Singapore
Singapore 117551, Singapore

J. Wang, Dr. K. A. Ulman, Prof. S. Y. Quek
Centre for Advanced 2D Materials
National University of Singapore
Block S14, Level 6, 6 Science Drive 2, Singapore 117546, Singapore

The ORCID identification number(s) for the author(s) of this article can be found under https://doi.org/10.1002/aelm.202000873.

DOI: 10.1002/aelm.202000873

Controlling carrier densities in semiconductors is essential for producing functional devices and can be achieved using various doping techniques. However, conventional doping methods, such as substitutional doping or ion implantation, do not work well for 2D materials that are being explored as alternative platforms for the next-generation of logic and memory devices.[1,2] Instead, owing to the high surface area, surface functionalization with organic electron donors (OEDs) is an effective approach to tune carrier density in 2D materials. This strategy has been successfully demonstrated in carbon nanotubes, graphene, and transition metal dichalcogenides for both electron and hole doping to generate materials with a wide range of doping levels.[3–21] For MoS_2 in particular,[22] the two-electron reduced form of benzyl viologen (BV^0) can dope MoS_2 degenerately with an electron sheet density of $\approx 1.2 \times 10^{13}$ cm^{-2}.

Despite the remarkable success of surface functionalization, a significant mismatch persists between the precision syntheses of OEDs with tailored structures and properties and our understanding of their doping efficiencies and effects on 2D materials. Accurate measurements of their doping powers are largely lacking, without which the full potential of OEDs as dopants cannot be realized through rational design. Here, we use monolayer MoS_2 flakes as a model system and measure the doping power of an organic dopant based on 4,4′-bis(dimethylamino) bipyridine (DMAP-OED),[23] which functionalizes the surface of MoS_2. The change in the carrier density after doping was measured by comparing the field-effect transistor (FET) characteristics of MoS_2 before and after functionalization, while the number of DMAP-OED molecules present on MoS_2 was quantified by X-ray photoelectron spectroscopy (XPS) and atomic force microscopy (AFM). We report a doping efficiency ranging between 0.63 and 1.26 electrons per molecule for DMAP-OED to MoS_2 and achieve a degenerate doping level with a carrier density of $5.8 \pm 1.9 \times 10^{13}$ cm^{-2} at the maximum functionalization conditions. This is four times greater than the best current system based on BV^0.[22] The doping levels achieved with DMAP-OED are well beyond those possible by field-effect gating and offer opportunities to access a wide range of electronic phases that are tuned by the electron density.[24]

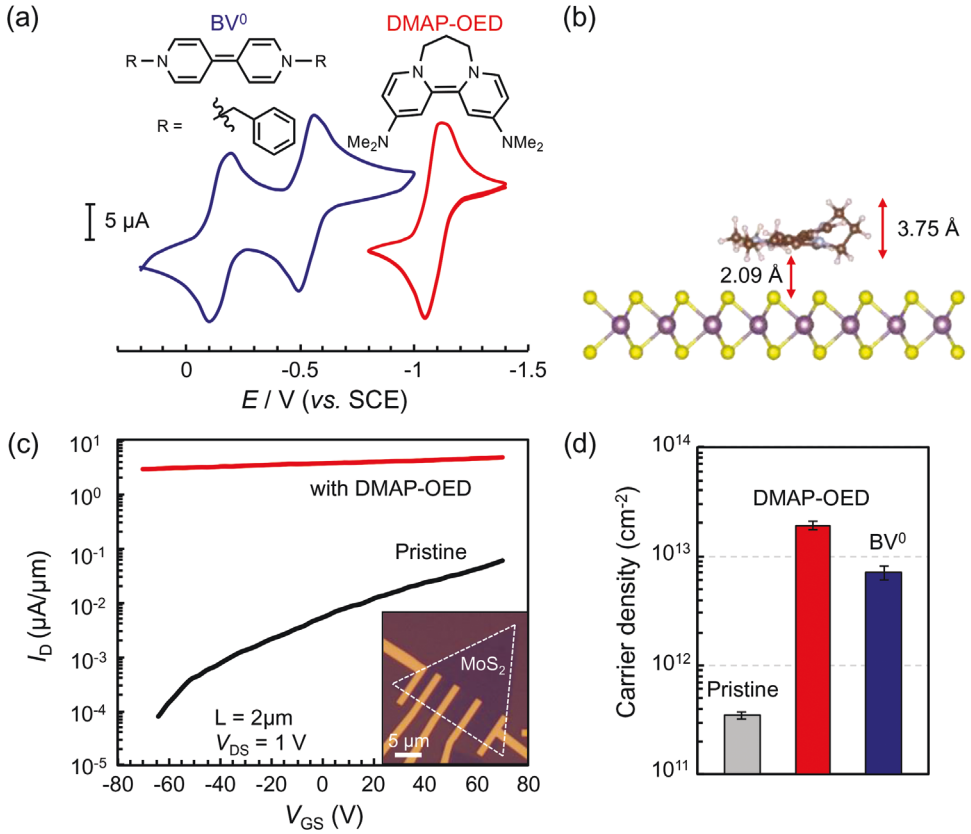

Figure 1. a) Chemical structures and CV scans of DMAP-OED and BV^0, indicating that DMAP-OED is a stronger reductant than BV^0. b) Atomic structure of a single DMAP-OED molecule on the surface of monolayer MoS_2. The aromatic rings of the DMAP-OED molecule are aligned parallel to the basal plane of MoS_2.c) Representative I_D–V_{GS} transfer curves of a pristine MoS_2 FET and after functionalization with a 10 mM DMAP-OED solution for 10 min. The *ID* at $V_{GS} = 0$ V increases by 3 orders of magnitude upon DMAP-OED doping and overall shows a weak gate dependency. The bias voltage is 1 V and the channel length is 2 μm. Inset: An optical image of the monolayer MoS_2 FET with various channel lengths. d) Average carrier densities at $V_{GS} = 0$ V for pristine (gray), DMAP-OED (red), and BV^0 (dark blue) functionalized MoS_2 FETs prepared using a 10 mM molecular solution and 10 min treatment time. The error bars in the carrier densities represent the standard error obtained from measuring 6 to 8 MoS_2 devices.

DMAP-OED is a neutral reductant which is stable and soluble in organic solvents under a nitrogen or argon atmosphere.[23] **Figure 1**a shows the molecular structures and cyclic voltammograms (CVs) of DMAP-OED and BV^0. The CV of DMAP-OED shows a single, reversible two-electron wave at –1.22 V versus the saturated calomel electrode (SCE). This reduction potential is significantly more negative than that of BV^0, which undergoes two discrete one-electron events at –0.33 and –0.72 V versus SCE. Based on their redox potentials, we hypothesized that DMAP-OED would be a stronger dopant for MoS_2 than BV^0. In agreement with the CV data, density functional theory (DFT) calculations indicate that a single DMAP-OED molecule adsorbed on a freestanding, monolayer MoS_2 (Figure 1b) should transfer 0.99 electrons to MoS_2, while a BV^0 molecule should transfer 0.69 electrons to MoS_2 in the same adsorption configuration (Figure S1, Supporting Information; Experimental Section).

Triangular flakes of monolayer MoS_2 were synthesized on Si/SiO_2 substrates by chemical vapor deposition (Figure S2, Supporting Information, and Experimental Section).[25] As-grown MoS_2 flakes were transferred to a fresh SiO_2 (285 nm) / Si (p^+) substrate and back-gated MoS_2 FETs were fabricated using standard e-beam lithography and e-beam evaporation of Ti/Au contacts (fabrication details in Experimental Section). For molecular doping, a 10 mM solution of DMAP-OED in acetonitrile was drop-cast on the MoS_2 FETs for 10 min inside an Ar-filled glove box. The devices were then rinsed with acetonitrile and dried under Ar. Figure 1c shows the representative transport characteristics of a MoS_2 FET before and after surface functionalization. In the pristine state, the width-normalized drain current (I_D) is $\approx 5.5 \times 10^{-3}$ μA/μm at zero gate voltage (V_{GS}), and the I_D versus V_{GS} shows typical *n*-type transport.[26,27] After surface functionalization with DMAP-OED, the I_D increases by 3 orders of magnitude to 3.6 μA/μm at $V_{GS} = 0$ V, and the threshold voltage (V_{th}) shifts to a more negative V_{GS}, indicating strong *n*-type doping. The average 2D sheet carrier densities (n_{2D}) of the pristine and functionalized MoS_2 were extracted from the transfer curves (Figure 1d) (See Figure S3, Supporting Information, and Experimental Section for details). The electron density increased from $3.5 \pm 0.3 \times 10^{11}$ to $1.9 \pm 0.2 \times 10^{13}$ cm^{-2} ($\Delta n_{2D} = 1.88 \times 10^{13}$ cm^{-2}) 1.88×10^{13} cm^{-2}) on average as a result of doping from DMAP-OED. The high carrier density achieved in the functionalized MoS_2 corresponds to its degenerate limit where the Fermi level lies inside the conduction band.[28]

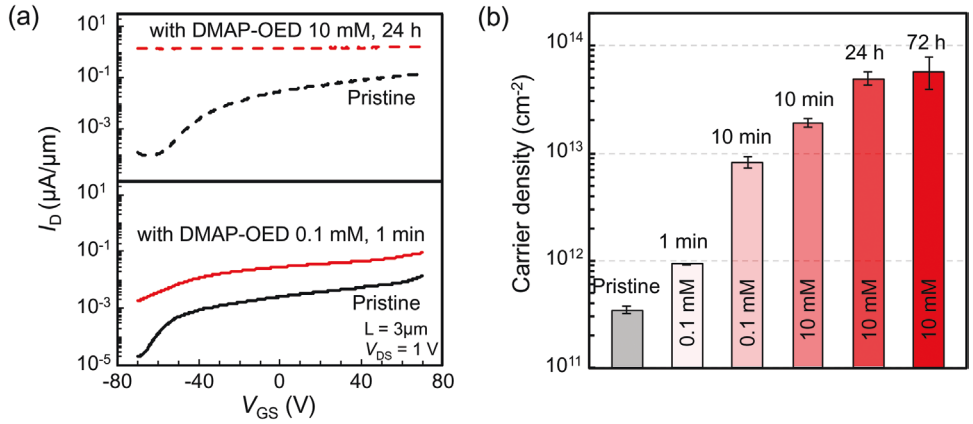

Figure 2. a) Representative I_D–V_{GS} transfer curves of MoS_2 FETs for two different DMAP-OED treatment conditions: (top) 10 mM, 24 h and (bottom) 0.1 mM, 1 min. The bias voltage is 1 V and the channel length of the devices is 3 μm. b) Systematic increase of the carrier density in MoS_2 at $V_{GS} = 0$ V with increasing DMAP-OED concentration and functionalization time.

As a control, we prepared a saturated solution of BV^0 in toluene and treated MoS_2 FETs for 10 min. The doping level achieved by the BV° functionalization is comparable to the reported values demonstrating that our method is consistent with other reported procedures.[22] As shown in Figure 1d, the average electron density of BV^0-functionalized MoS_2 is three times lower than that of DMAP-OED-functionalized MoS_2. The lower doping power of BV° compared to DMAP-OED agrees with the relative redox potentials of the two molecules (Figure 1a) as well as with their calculated doping powers. Additionally, control experiments show that the high *n*-type doping observed in the DMAP-OED-functionalized MoS_2 is not due to the acetonitrile solvent (Figure S4, Supporting Information), nor to the formation of a continuous film of DMAP-OED that might contribute to electrical current (Figure S5, Supporting Information).

Figure 2 shows the systematic increase in the carrier density of MoS_2 as the functionalization conditions were varied. Representative FET measurements for two different functionalization conditions are shown in Figure 2a, which demonstrate that when MoS_2 is exposed to a DMAP-OED solution of higher concentration for a longer time there is a greater increase in I_D, which indicates stronger electron doping. Figure 2b provides a summary of FET measurements using various functionalization conditions, plotted in order of increasing average carrier density. As expected, increasing the treatment time or the concentration of DMAP-OED in solution increases the electron density of MoS_2; this can be attributed to more DMAP-OED molecules being present on the surface of MoS_2, which leads to higher *n*-type doping. In the case of a 10 mM DMAP-OED solution and an exposure time of 72 h, the carrier density saturates at $\approx 5.8 \pm 1.9 \times 10^{13}$ cm^{-2}, representing the highest doping level achieved among all of the reported values of molecular doping in MoS_2 using organic or organometallic molecules.[14–18,20,22]

The electron transfer from DMAP-OED to MoS_2 was further examined using XPS. **Figure 3**a,b show the Mo *3d* and S *2p* peaks of the pristine and functionalized MoS_2 using a 10 mM DMAP-OED solution and an exposure time of 10 min. After surface functionalization, the binding energies of the Mo and S core levels decrease by ≈0.6 and 0.5 eV, respectively, which indicates electron transfer from DMAP-OED to MoS_2, resulting in lower oxidation states of Mo and S.[29] The line shape of the XPS peaks did not change after functionalization, suggesting physisorption of DMAP-OED molecules on the surface of the MoS_2. Similar downshifts of the core level peaks were observed for functionalization of MoS_2 with BV^0 (Figure S6, Supporting Information). Systematic XPS characterizations as a function of functionalization conditions are tabulated in Table S1, Supporting Information. We also performed Raman spectroscopy and photoluminescence (PL) measurements on MoS_2 before and after DMAP-OED functionalization (Figure S7, Supporting Information). Structurally MoS_2 remains in the semiconducting 2H phase while the PL intensity decreases significantly with increase in the trion peak relative to the exciton peak after functionalization in accordance with electron doping effects on MoS_2.[30,31]

To measure the doping power of each DMAP-OED molecule to MoS_2, the measured increase in the carrier density must be divided by the number of dopant molecules on the MoS_2 surface. We quantitatively measured the number of DMAP-OED molecules on MoS_2 by examining the XPS N *1s* peak as the dopant molecule contains 4 nitrogen atoms (Figure 3c). The N *1s* peak is absent in the pristine MoS_2, confirming its origin from DMAP-OED. By comparing the relative areas of the N and Mo peaks, a ratio of 1 DMAP-OED per 3.85 Mo atoms is obtained for MoS_2 functionalized with a 10 mM DMAP-OED solution for 10 min. Assuming a lattice constant of 3.16 Å for 2H-MoS_2,[32] a surface density of 3×10^{14} molecule cm^{-2} was determined for DMAP-OED on MoS_2. For functionalization with BV^0, approximately three times as many BV^0 molecules were estimated to be on the surface of MoS_2 with a density of 9.6×10^{14} molecule cm^{-2} under similar functionalization conditions (Table S1, Supporting Information). This is consistent with the smaller size of BV^0.

Given that the increase in the carrier density was $1.88 \pm 0.2 \times 10^{13}$ cm^{-2} for the 10 mM DMAP-OED solution with 10 min treatment time, the XPS analysis suggests that the doping power of DMAP-OED is ≈0.06 electron per molecule, which is far lower than the prediction from DFT calculations as well as what is

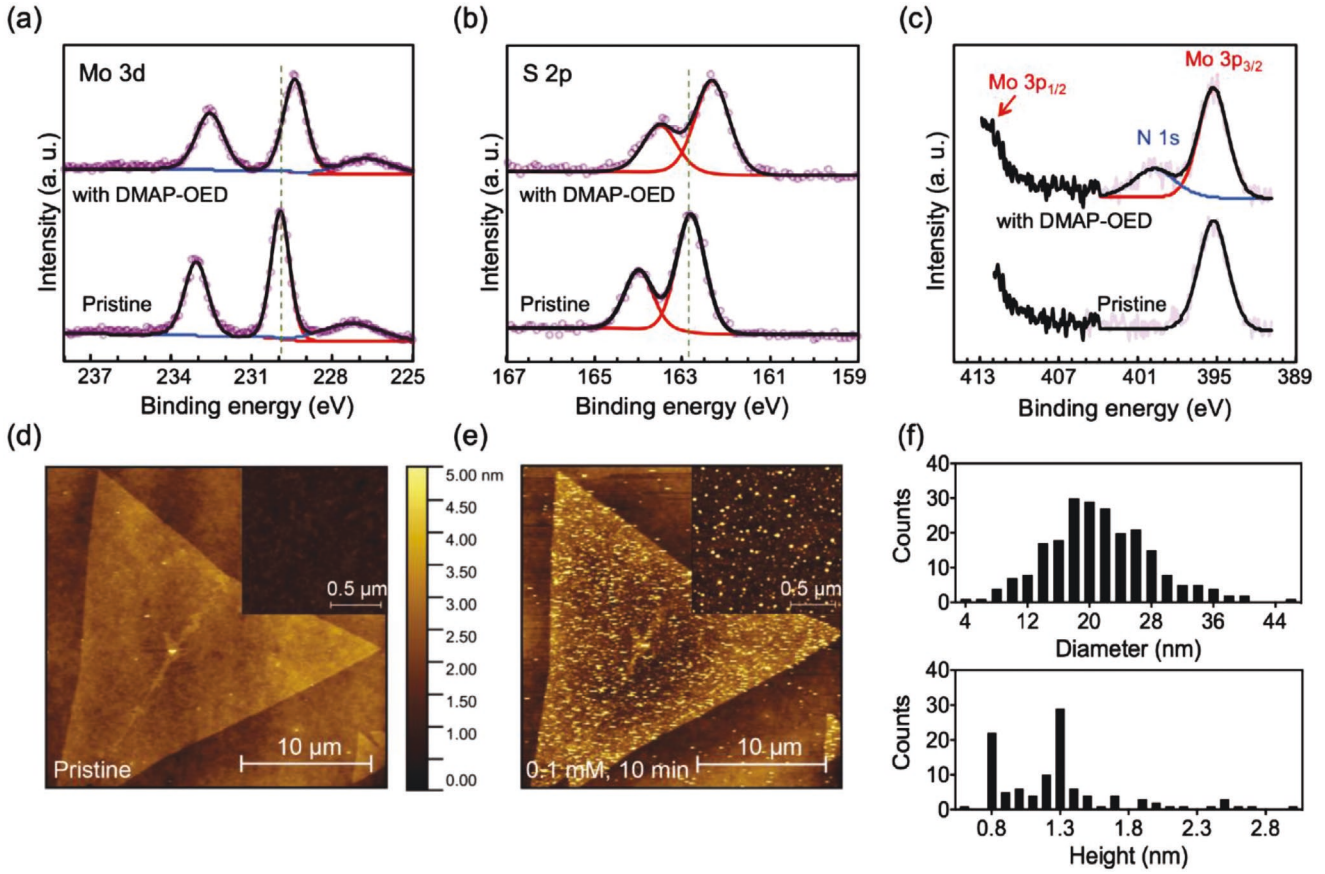

Figure 3. XPS spectra of a) Mo *3d*, b) S *2p*, and c) N *1s* core levels before and after treating MoS_2 with a 10 mM DMAP-OED solution for 10 min. The downshift of the binding energies of the pristine peaks, indicated by the green dashed lines in (a) and (b), confirms lower oxidation states of Mo and S due to electron injection into MoS_2. AFM images of d) pristine and e) DMAP-OED-functionalized MoS_2 after treating MoS_2 with a 0.1 mM DMAP-OED solution for 10 min. Insets: Zoom-in AFM images. As revealed by the bright spots in (e) DMAP-OED tends to aggregate and form islands. f) Diameter and height distributions of the molecule islands formed on MoS_2 after functionalization with a 0.1 mM DMAP-OED solution for 10 min.

expected based on the redox potential of DMAP-OED. The lateral dimensions of a DMAP-OED molecule are about 0.97 nm × 1.08 nm, which is approximately twelve times larger than the unit cell of MoS_2. Therefore, a DMAP-OED molecule with its aromatic rings aligned parallel to the surface of MoS_2 would cover 12 Mo atoms, which suggests that the estimated ratio of 1 DMAP-OED per 3.85 Mo atoms from XPS indicates formation of multi-layer islands or films where molecules are stacked on top of each other. Since the doping power of the molecule is expected to decrease as it moves away from the surface of MoS_2, we estimate that not all the molecules measured by XPS are donating electrons equally to MoS_2.

The results described above suggest that when MoS_2 is functionalized with a 10 mM DMAP-OED solution for 10 min, a "saturated" system in which many of the molecules are not donating electrons to MoS_2 is obtained. Thus, we examined the functionalization condition of a 0.1 mM DMAP-OED solution for 10 min. In this case, we could not use XPS to quantitatively measure the surface density of DMAP-OED on MoS_2 as the N *1s* peak was not clearly resolved after surface functionalization (Figure S6, Supporting Information). We thus used AFM to estimate the molecule surface coverage and determine the doping power of DMAP-OED. Figure 3d,e show the AFM images of pristine and functionalized MoS_2 treated with a 0.1 mM DMAP-OED solution for 10 min, which show that the molecules aggregate and form islands. Analysis of AFM images shows an average areal coverage of 11% for functionalized MoS_2. The surface roughness of the uncovered areas is comparable to that of the pristine MoS_2, indicating that only the islands contain the molecules. Over 200 islands were analyzed to obtain the diameter and height distributions of the islands (Figure 3f). A striking number of the islands are either ≈0.8 or 1.3 nm in height, while they are broadly distributed in diameter with an average value of 21.4 ± 0.7 nm. Accounting for the height of the DMAP-OED molecule (0.375 nm, Figure 1b), the space between the molecule and MoS_2 (0.209 nm), and the interlayer spacing between the molecules, the observed heights of 0.8 and 1.3 nm strongly suggest that the islands are either mono- or bi-layer islands. The surface coverage of DMAP-OED decreases to ≈1.6 % with mainly monolayer islands when the functionalization time was shortened to 1 min (Figure S8, Supporting Information). We note that MoS_2 treated only with acetonitrile showed less than ≈0.2 % areal coverage of small islands, eliminating the possibility that the islands are from the solvent molecules.

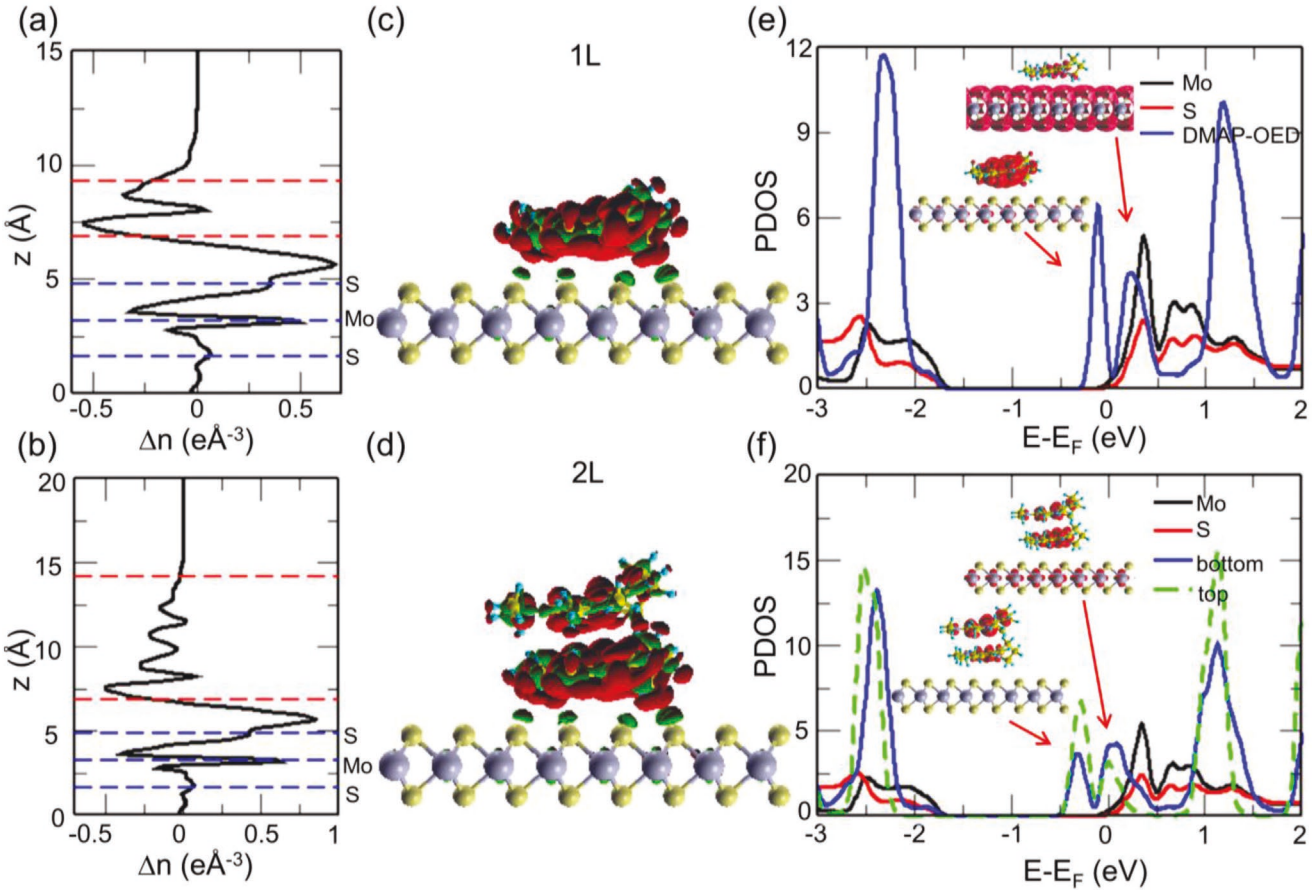

Figure 4. The planar-averaged differential charge density Δn (e Å^{-3}) of a) 1-layer (1L) and b) 2-layer (2L) configurations. Blue dashed lines correspond to Mo and S atomic layers while red dashed lines denote the upper and lower boundaries of the molecules. Differential charge density $\Delta\rho$ of c) 1L and d) 2L configurations. The differential charge density is defined as $\Delta\rho = \rho_{mol/MoS_2} - \rho_{MoS_2} - \rho_{mol}$. Electron depletion and accumulation are indicated by red and green colors, respectively. The iso-value is 5% of the maximum value. PDOS for e) 1L and f) 2L configurations. The PDOS shown here is the sum of spin up and spin down PDOS (see Figure S10, Supporting Information, for spin-polarized PDOS). The PDOS on MoS_2 is divided by 64 for clarity. The partial charge densities of selected peaks in the molecular PDOS are shown as insets (the iso-value is 1% of the maximum value in (e) and 5% of the maximum value in (f)).

To calculate the doping power of a DMAP-OED molecule from the AFM data that shows mono- and bi-layer islands, we consider two scenarios: the first is electron doping by only the first layer of molecules closest to MoS_2 and the second is electron doping by both layers of molecules with equal doping power. We focus on the case of a 0.1 mM DMAP-OED solution functionalizing MoS_2 for 10 min. Based on the AFM results (Figure 3d–f), the total number of DMAP-OED molecules in the first and second layer is estimated to be 1.25×10^{13} molecules cm^{-2} (Supporting Information). Given the change in the carrier density of $7.9 \pm 1.0 \times 10^{12}$ cm^{-2} (Figure 2b), the estimated doping power of a single DMAP-OED molecule to MoS_2 is 1.26 ± 0.15 electrons per molecule in the first scenario and 0.63 ± 0.08 electron per molecule in the second scenario. The doping power of DMAP-OED is on a similar order when the functionalization time is shortened to 1 min, given the ten times reduction in both the surface coverage and induced carrier density. Thus we observe a near unity doping efficiency for DMAP-OED to MoS_2.

DFT calculations were performed to provide further understanding of our results. **Figure 4** shows the calculated electronic structure of DMAP-OED-functionalized MoS_2 for two cases: a single DMAP-OED molecule in an 8×8 MoS_2 supercell (1-layer (1L); Figure 4a,c,e) and two molecules vertically stacked on MoS_2 in the same supercell (2-layer (2L); Figure 4b,d,f). Electrons from the molecules are transferred predominantly to the interfacial region and Mo sites (Figure 4a,b, and Figure S9, Supporting Information). These electrons are donated from the highest occupied molecular orbital (HOMO) of DMAP-OED. In the 1L case, the HOMO becomes approximately half-unoccupied and splits into two non-degenerate spin-polarized orbitals (Figure 4e). The calculated doping power is 0.99 electrons per molecule to MoS_2 (Experimental Section). In the 2L case, the HOMOs of the two molecules hybridize and split into two peaks in the projected density of states (PDOS) (Figure 4f). One of the peaks is primarily localized on the top molecule and remains fully occupied after functionalization, while the other peak is primarily localized on the bottom molecule and becomes partially unoccupied (Figure 4f). The two molecules donate a total of 1.27 electrons to MoS_2, with the molecule in direct

Table 1. Calculated number of electrons donated from each DMAP-OED molecule to monolayer MoS_2, in different atomic configurations. The 1L configuration has one molecule in an 8×8 MoS_2 supercell (Figure 4c), while the 2L configuration has two molecules stacked on top of one another in an 8×8 MoS_2 supercell (Figure 4d). The "1L denser coverage" configuration has two molecules arranged side by side in an 8×8 MoS_2 supercell (Figure S9e, Supporting Information), while the "2L denser coverage" configuration has four molecules in total in two layers where each layer has two molecules arranged side by side in an 8×8 MoS_2 supercell (Figure S9f, Supporting Information). All atomic configurations are shown in Figure S1, Supporting Information.

Configurations	1L [1 molecule]	2L [2 molecules]	1L denser coverage [2 molecules]	2L denser coverage [4 molecules]
Molecule in 1st layer (in direct contact with MoS_2)	0.99	0.86	0.89/0.89	0.74/0.74
Molecule in 2nd layer	/	0.41	/	0.24/0.24

contact with MoS_2 donating 0.86 electrons. These calculated doping powers are in good agreement with the experimental results. Further, the calculations show that increasing the surface coverage of DMAP-OED molecules by arranging two molecules side by side on MoS_2 (Figure S1, Supporting Information) reduces the doping power per molecule, while the total charge donated by the molecules to MoS_2 increases. **Table 1** summarizes the doping powers of DMAP-OED molecules with four different configurations in relation to MoS_2, and shows diminishing doping power per molecule for higher coverage. We note that the Fermi levels of the DMAP-OED-functionalized MoS_2 are within the conduction band of MoS_2 (Figure 4e,f), consistent with the degenerate electron-doping observed experimentally. In the presence of a sulfur vacancy in MoS_2 (Figure S1, Supporting Information), we calculate that the doping power of DMAP-OED increases to 1.27 electrons per molecule in the 1L case, suggesting that the nature of MoS_2 can significantly influence doping efficiencies of DMAP-OED.

In conclusion, the ability to dope MoS_2 beyond its degenerate limit via an organic super electron donor provides opportunities to access correlated electronic phases, such as superconductivity at the degenerate level, and provides an alternative to ionic gating. Using DMAP-OED, we have demonstrated a record molecular doping level in monolayer MoS_2. Further, we established that a single DMAP-OED molecule donates 0.63–1.26 electrons per molecule to MoS_2, one of the first evaluations of the doping power of an OED. We observe that DMAP-OED aggregates and forms islands on MoS_2, which eventually limits the doping efficiency. Altogether, we establish that multiple factors, such as reduction potential, size, and binding mode of the dopant molecule, as well as interactions between the molecules and 2D materials and among the molecules themselves play an important role when considering the design of strong molecular dopants. In fact, forming a uniform dopant layer whereby all molecules contribute equally to doping should result in the doping efficiencies exceeding the values reported here. Overall, our findings provide insight to guide the development of strongly doped 2D materials.

Experimental Section

Synthesis and Characterization of DMAP-OED and BV^0: DMAP-OED was synthesized according to a literature procedure.[33] The ^{1}H NMR spectrum was consistent with that previously reported and the solid was stored under an N_2 or Ar atmosphere. BV^0 was synthesized according to the following procedure:

To a 500 mL Schlenk flask in a glovebox under an N_2 atmosphere was added benzyl viologen dibromide (3.3 g, 6.75 mmol), magnesium powder (0.51 g, 20.25 mmol), and acetonitrile (30 mL). The Schlenk flask was sealed and removed from the glovebox and it was allowed to stir at 60 °C for five days. Initially, the reaction was a yellow suspension. After 30 min, the solution began to turn deep blue. The blue color deepened and the yellow precipitate disappeared over days. After five days, a red solution and red precipitate were present. The reaction flask was allowed to cool to room temperature and volatiles were removed under vacuum. The crude solid was taken up in 250 mL of THF and filtered under N_2, then the volatiles were removed under vacuum. The remaining solid was washed with room temperature ethanol (3×20 mL) under N_2 and then dried overnight under vacuum to afford BV^0 as a dark red solid, which was stored under an N_2 atmosphere (400 mg, 18%). ^{1}H NMR (500 MHz, THF-d_8) δ 7.29–7.28 (m, 8H), 7.22–7.19 (m, 2H), 5.71 (b, 4H), 5.25 (b, 4H), 4.19 (b, 4H). For the ^{1}H NMR spectrum of BV^0, see Figure S11, Supporting Information.

Benzyl viologen dibromide was synthesized according to a literature procedure.[34] Magnesium powder was activated by stirring it in tetrahydrofuran at 40 °C with 0.025 equivalents of 1,2-dibromoethane for 1 h under a stream of N_2 with a gas outlet because the reaction evolves ethylene. The solid was then collected via filtration and washed further with tetrahydrofuran under an N_2 atmosphere. The solid was dried under vacuum and stored under an N_2 atmosphere.

Acetonitrile used for synthesis of BV^0 and MoS_2 functionalization was purchased from Honeywell (Cat. No. CS017-56) and used without further purification.

CVD Synthesis of MoS_2: Monolayer MoS_2 flakes were synthesized on SiO_2/Si substrates in a 1-inch quartz tube furnace. ≈0.4 mg of MoO_3 powder was placed in a quartz crucible at the center of the furnace, and ≈200 mg of sulfur powder was placed upstream in an alumina crucible liner, with 17 cm separating the precursors. A 285 nm SiO_2/Si substrate was treated with piranha solution (3:1 H_2SO_4 : H_2O_2) for at least 1 h, and subsequently rinsed with deionized water and dried using a stream of N_2 gas. The substrate was then treated with a single drop (≈4 µL) of 100 µM perylene-3,4,9,10 tetracarboxylic acid tetrapotassium salt (PTAS). After drying the PTAS-treated substrate on a hot plate in air, the substrate was placed face down on the MoO_3 crucible. The quartz tube was purged several times with ultra-high purity Ar gas to ensure no residual oxygen was present. The furnace temperature was ramped to 850 °C, and then kept at 850 °C for 15 min, while flowing Ar at ≈10 sccm. After the reaction, the furnace was naturally cooled to 580 °C, and then the lid was opened to accelerate the cooling to room temperature. Raman spectroscopy, PL, AFM, and time-of-flight secondary ion mass spectrometry were utilized to confirm that the MoS_2 is a monolayer with uniform distributions of S and Mo (see Figure S2, Supporting Information).

Device Fabrication and Characterization: To avoid gate leakage, the as-grown MoS_2 monolayers were transferred to a fresh SiO_2 (285 nm) / Si (p^+) substrate, which served as back-gate for field-effect devices. For the transfer of MoS_2, 950 PMMA A4 (MicroChem) was spin-coated on the growth SiO_2 substrates containing MoS_2 flakes and baked at 120 °C for 5 min on a hot plate. The PMMA / MoS_2 film was released from the SiO_2 substrate by floating the sample in 2 M KOH at 65 °C for 1 h. The film was then rinsed with deionized water several times and transferred to a fresh SiO_2 / Si substrate. After drying the sample on a hot plate at 40 °C for 40 min, the sample was kept in acetone overnight to remove the PMMA. Electron beam lithography was used to pattern the metal contacts followed by e-beam evaporation of Ti (10 nm) / Au (60 nm) and lift-off in acetone overnight. Electrical measurements were performed on these devices before and after molecular functionalization. The electrical characteristics of the devices were measured in air using a semiconductor device analyzer (Agilent Technologies B1500A).

Carrier Density Calculation: From the FET transfer curves, the 2D sheet carrier density in MoS_2 was calculated by $n_{2D} = (I_D L)/(qWV_{DS}\mu)$,[22] where I_D is the drain current at the zero gate voltage; L and W are the length and width of the channel, respectively; q is the electron charge, and μ is the field-effect mobility at $V_{DS} = 1$ V. The mobility was calculated as $\mu = ((\partial I_D/\partial V_{GS})\, L/(V_{DS}C_{ox}W))$, where $(\partial I_D/\partial V_{GS})$ is the maximum transconductance (see Figure S3, Supporting Information), and C_{ox} is the gate capacitance of 1.2×10^{-8} F cm^{-2} for 285 nm thick SiO_2 estimated based on the parallel-plate model. Numerous MoS_2 devices were measured to ensure reproducibility of the observed transfer curves and to obtain the average n_{2D} and the standard error, which represent the error bars (Figures 1d and 2b).

XPS, PL, and Raman Characterization: XPS was performed on a PHI VersaProbe II Scanning XPS Microprobe with an Al K_α monochromatic X-ray source. In order to prevent exposure of samples to the ambient environment, a vacuum vessel was used to transfer the samples from a glovebox to the XPS instrument. A beam spot with the diameter of 20 µm was used to obtain XPS data only from the MoS_2 flakes, assisted by scanning X-ray induced secondary electron imaging. All of the XPS spectra were calibrated using a carbon 1s peak located at 284.50 eV. PL and Raman measurements were conducted on a Horiba LabRAM HR Evolution Raman system with a 532 nm laser.

AFM Characterization: AFM images were acquired with a Cypher ES Environmental AFM System (Asylum Research Oxford Instruments) in tapping mode using the FS-1500AuD (Asylum Research Oxford Instruments) cantilever at a scan rate between 4.88 and 7.81 Hz. All imaging was performed in ambient conditions. To determine the surface coverage of DMAP-OED on functionalized flakes, AFM images were acquired from several scanning areas and with at least five different scan sizes between 500 nm and 5 µm. Images were also acquired from pristine MoS_2 flakes to determine their root-mean-square (RMS) surface roughness at a scan size of 500 nm. The RMS surface roughness of the uncovered areas of functionalized flakes was equivalent to that of the pristine MoS_2 surface, which confirms the absence of any molecules in these areas. The images were processed using ImageJ to set a background threshold, perform particle analysis, and calculate the percent surface coverage. For each set of functionalization conditions, the same analysis was performed for 15 samples and the results were averaged.

DFT Calculations: Spin-polarized DFT calculations for all functionalized MoS_2 monolayers were performed using the SIESTA code,[35] with the generalized gradient approximation[36] for the exchange-correlation functional. The semi-empirical DFT-D2 method of Grimme[37] was used to describe the van der Waals interactions. Norm-conserving Troullier–Martins pseudopotentials with partial core corrections were used. Double-zeta plus polarization basis sets (details in Supporting Information) were chosen to reproduce the experimental work function of MoS_2 and the trends in gas phase energy levels were predicted using Gaussian 16 (see Supporting Information). The Brillouin zone was sampled by a $3 \times 3 \times 1$ k-point grid. A mesh cutoff energy of 300 Ry was used to obtain the electronic wavefunctions and charge densities. Atomic positions were relaxed until the forces were smaller than 0.02 eV Å^{-1}. For calculating the doping power of the organic reductants, Bader charge analysis[38] was performed using a fine FFT mesh of $240 \times 240 \times 960$, which was sufficient to achieve convergence. A finer k-point grid of $12 \times 12 \times 1$ and a Gaussian broadening of 0.08 eV were used to obtain the PDOS.

Supporting Information

Supporting Information is available from the Wiley Online Library or from the author.

Acknowledgements

M.Y. and Y.Z. contributed equally to this work. M.Y. acknowledges support from the Army Office of Research (W911NF-18-1-0367) for the device fabrication and FET measurements of surface-functionalized MoS_2. Synthesis of MoS_2 flakes was supported by NSF CAREER 1749742. Y.Z. acknowledges the Link Foundation energy fellowship. S.N.R. acknowledges the Ford Foundation for a graduate student fellowship. H.W. and N.H. acknowledge support of a seed grant from the Center for Research on Interface Structures and Phenomena at Yale University. J.B.C. thanks the NSF for the graduate research fellowship. Material characterizations were carried out at shared facilities including Yale West Campus Materials Characterization Core, the Yale Institute for Nanoscience and Quantum Engineering, and the School of Engineering Cleanroom. S.Y.Q., J.W., and K.A.U. acknowledge funding from Grant MOE2016-T2-2-132 from the Ministry of Education, Singapore, and support from the Singapore National Research Foundation, Prime Minister's Office, under its medium-sized center program. Computations were performed on the NUS Graphene Research Centre cluster and National Supercomputing Centre Singapore.

Conflict of Interest

The authors declare no conflict of interest.

Keywords

molecular doping, MoS_2, organic electron donors, surface functionalization, transition metal dichalcogenides

Received: September 2, 2020
Revised: November 12, 2020
Published online:

[1] D. Akinwande, C. Huyghebaert, C. H. Wang, M. I. Serna, S. Goossens, L. J. Li, H.-S. P. Wong, F. H. L. Koppens, *Nature* **2019**, *573*, 507.
[2] S. Bertolazzi, M. Gobbi, Y. Zhao, C. Backes, P. Samori, *Chem. Soc. Rev.* **2018**, *47*, 6845.
[3] P. Wei, N. Liu, H. R. Lee, E. Adijanto, L. Ci, B. D. Naab, J. Q. Zhong, J. Park, W. Chen, Y. Cui, Z. Bao, *Nano Lett.* **2013**, *13*, 1890.
[4] S. Y. Zhou, D. A. Siegel, A. V. Fedorov, A. Lanzara, *Phys. Rev. Lett.* **2008**, *101*, 086402.
[5] S. M. Kim, J. H. Jang, K. K. Kim, H. K. Park, J. J. Bae, W. J. Yu, H. Lee, G. Kim, D. D. Loc, U. J. Kim, E. H. Lee, H. J. Shin, J. Y. Choi, Y. H. Lee, *J. Am. Chem. Soc.* **2009**, *131*, 327.
[6] J. Park, S. B. Jo, Y. J. Yu, Y. Kim, J. W. Yang, W. H. Lee, H. H. Kim, B. H. Hong, P. Kim, K. Cho, K. S. Kim, *Adv. Mater.* **2012**, *24*, 407.
[7] W. Zhang, C. T. Lin, K. K. Liu, T. Tite, C. Y. Su, C. H. Chang, Y. H. Lee, C. W. Chu, K. H. Wei, J. L. Kuo, L. J. Li, *ACS Nano* **2011**, *5*, 7517.
[8] S. Y. Lee, D. L. Duong, Q. A. Vu, Y. Jin, P. Kim, Y. H. Lee, *ACS Nano* **2015**, *9*, 9034.
[9] W. J. Yu, L. Liao, S. H. Chae, Y. H. Lee, X. F. Duan, *Nano Lett.* **2011**, *11*, 4759.
[10] K. Cho, J. Pak, S. Chung, T. Lee, *ACS Nano* **2019**, *13*, 9713.
[11] Y. L. Huang, Y. J. Zheng, Z. Song, D. Chi, A. T. S. Wee, S. Y. Quek, *Chem. Soc. Rev.* **2018**, *47*, 3241.
[12] M.-A. Stoeckel, M. Gobbi, T. Leydecker, Y. Wang, M. Eredia, S. Bonacchi, R. Verucchi, M. Timpel, M. V. Nardi, E. Orgiu, P. Samori, *ACS Nano* **2019**, *13*, 11613.
[13] M. Gobbi, E. Orgiu, P. Samori, *Adv. Mater.* **2018**, *30*, 1706103.
[14] S. Zhang, H. M. Hill, K. Moudgil, C. A. Richter, A. R. H. Walker, S. Barlow, S. R. Marder, C. A. Hacker, S. J. Pookpanratana, *Adv. Mater.* **2018**, *30*, 1802991.

[15] R. Guo, Q. Li, Y. Zheng, B. Lei, H. Sun, Z. Hu, J. Zhang, L. Wang, E. Longhi, S. Barlow, S. R. Marder, J. Wang, W. Chen, *Mater. Today* **2019**, *30*, 26.
[16] S. Najmaei, X. Zou, D. Er, J. Li, Z. Jin, W. Gao, Q. Zhang, S. Park, L. Ge, S. Lei, J. Kono, V. B. Shenoy, B. I. Yakobson, A. George, P. M. Ajayan, J. Lou, *Nano Lett.* **2014**, *14*, 1354.
[17] A. Tarasov, S. Zhang, M. Y. Tsai, P. M. Campbell, S. Graham, S. Barlow, S. R. Marder, E. M. Vogel, *Adv. Mater.* **2015**, *27*, 1175.
[18] L. Yang, K. Majumdar, H. Liu, Y. Du, H. Wu, M. Hatzistergos, P. Y. Hung, R. Tieckelmann, W. Tsai, C. Hobbs, P. D. Ye, *Nano Lett.* **2014**, *14*, 6275.
[19] H. G. Ji, P. S. Fernandez, D. Yoshimura, M. Maruyama, T. Endo, Y. Miyata, S. Okada, H. Ago, *Adv. Mater.* **2019**, *31*, 1903613.
[20] K. Cho, J. Pak, J. K. Kim, K. Kang, T. Y. Kim, J. Shin, B. Y. Choi, S. Chung, T. Lee, *Adv. Mater.* **2018**, *30*, 1705540.
[21] X. Zhang, Z. Shao, X. Zhang, Y. He, J. Jie, *Adv. Mater.* **2016**, *28*, 10409.
[22] D. Kiriya, M. Tosun, P. Zhao, J. S. Kang, A. Javey, *J. Am. Chem. Soc.* **2014**, *136*, 7853.
[23] J. A. Murphy, J. Garnier, S. R. Park, F. Schoenebeck, S. Zhou, A. T. Turner, *Org. Lett.* **2008**, *10*, 1227.
[24] B. Radisavljevic, A. Kis, *Nat. Mater.* **2013**, *12*, 815.
[25] K. K. H. Smithe, C. D. English, S. V. Suryavanshi, E. Pop, *2D Mater.* **2017**, *4*, 011009.
[26] Y. Liu, J. Guo, E. Zhu, L. Liao, S. J. Lee, M. Ding, I. Shakir, V. Gambin, Y. Huang, X. Duan, *Nature* **2018**, *557*, 696.
[27] S. Das, H.-Y. Chen, A. V. Penumatcha, J. Appenzeller, *Nano Lett.* **2013**, *13*, 100.
[28] K. Kaasbjerg, K. S. Thygesen, K. W. Jacobsen, *Phys. Rev. B* **2012**, *85*, 115317.
[29] H. Wang, Z. Lu, S. Xu, D. Kong, J. J. Cha, G. Zheng, P. C. Hsu, K. Yan, D. Bradshaw, F. B. Prinz, Y. Cui, *Proc. Natl. Acad. Sci. USA* **2013**, *110*, 19701.
[30] S. Mouri, Y. Miyauchi, K. Matsuda, *Nano Lett.* **2013**, *13*, 5944.
[31] Y. Wang, S. M. Gali, A. Slassi, D. Beljonne, P. Samori, *Adv. Funct. Mater.* **2020**, *30*, 2002846.
[32] D. Voiry, R. Fullon, J. Yang, C. Silva, R. Kappera, I. Bozkurt, D. Kaplan, M. J. Lagos, P. E. Batson, G. Gupta, A. D. Mohite, L. Dong, D. Er, V. B. Shenoy, T. Asefa, M. Chhowalla, *Nat. Mater.* **2016**, *15*, 1003.
[33] J. Broggi, M. Rollet, J. L. Clement, G. Canard, T. Terme, D. Gigmes, P. Vanelle, *Angew. Chem., Int. Ed.* **2016**, *55*, 5994.
[34] Y. Zhang, K. Liu, L. Wu, H. Zhong, N. Luo, Y. Zhu, M. Tong, Z. Long, G. Chen, *ACS Sustainable Chem. Eng.* **2019**, *19*, 16907.
[35] J. M. Soler, E. Artacho, J. D. Gale, A. Garcia, J. Junquera, P. Ordejon, D. S. Portal, *J. Phys.: Condens. Matter* **2002**, *14*, 2745.
[36] J. P. Perdew, K. Burke, M. Ernzerhof, *Phys. Rev. Lett.* **1996**, *77*, 3865.
[37] S. Grimme, *J. Comput. Chem.* **2006**, *27*, 1787.
[38] R. F. W. Bader, *Acc. Chem. Res.* **1985**, *18*, 9.

